J. Phys. D: Appl. Phys. **41** (2008) 095111 (7pp) doi:10.1088/0022-3727/41/9/095111

Photoacoustic imaging using an ultrasonic Fresnel zone plate transducer

Hui Wang, Da Xing[1] and Liangzhong Xiang

MOE Key Laboratory of Laser Life Science and Institute of Laser Life Science, South China Normal University, Guangzhou 510631, People's Republic of China

E-mail: xingda@scnu.edu.cn

Received 8 December 2007, in final form 4 March 2008
Published 7 April 2008
Online at stacks.iop.org/JPhysD/41/095111

Abstract

A photoacoustic (PA) imaging system based on an ultrasonic Fresnel zone plate (FZP) transducer is developed for the purpose of imaging biological tissue. This FZP transducer has a two-zone negative zone plate piezoelectric material pattern, and an optical fibre is integrated with the transducer on the symmetric axis of the zone plates to deliver laser pulses to the sample. The focal characteristic of the FZP transducer is analysed by theoretical prediction and experimental measurement, and the measured results are in good agreement with the predicted results. The limited-field back-projection deconvolution algorithm combined with the coherence-factor weighting technique is used to reconstruct the optical absorption distribution. The experiments were performed with phantoms and the blood vessels of chicken embryo chorioallantoic membrane. The results demonstrate that PA imaging using the FZP transducer has the ability to image biological tissue and has potential application in monitoring neovascularization in tumour angiogenesis.

1. Introduction

In recent years, there has been wide interest in developing new techniques for non-invasive imaging of biological tissue. Photoacoustic (PA) imaging is an ideal candidate because this hybrid technique combines the high intrinsic contrast of optical imaging and the high spatial resolution of pure ultrasound imaging. It is non-invasive and non-destructive and does not rely on the use of ionizing radiation. This technique is based on the detection of acoustic waves generated by absorption of pulsed light by tissue chromophores. Because the initial ultrasonic pressure is proportional to the local optical energy deposition in tissue, the induced acoustic signals exhibit heterogeneity of optical absorption in tissue and the PA imaging reveals the optical absorption distribution of tissue.

Due to its high optical absorption contrast and low ultrasound scattering, PA imaging has been applied to *in vivo* imaging of subcutaneous vasculature in small animals and humans [1–5], detecting early breast tumors or cancer [6–8]. The PA technique has also been used for non-invasive monitoring of blood oxygenation (especially cerebral oxygenation) and cerebrovascular activities in small animals [9–11], monitoring of vascular damage during tumour photodynamic therapy [12] and monitoring of skin abnormalities [13, 14]. In most imaging systems, the imaging mode with the transducer circularly scanning the sample determines that these imaging systems can only be used to detect the prominent parts of the body, such as brain and breast. In this paper, we have developed a PA imaging system based on an ultrasonic Fresnel zone plate (FZP) transducer to image biological tissue. This FZP transducer operates in reflection mode, and it allows scanning in a line or a plane. This scanning mode is more flexible than the traditional circular scanning mode, so it can be applied to various sites of the body to image absorption structures like blood vessels or tumors *in vivo*.

The classical FZP, which has been extensively used in the field of optics [15], has also been utilized successfully in acoustics imaging system as a means of focusing water-coupled or air-coupled ultrasonic transducers for its good focusing effect [16, 17]. However, the FZP has not been applied to PA imaging system to our knowledge. We use a FZP transducer in the PA imaging system to image biological tissue for the first time.

A zone plate is a mask with a sequence of alternately transparent and opaque zones. The transparent zones allow

[1] Author to whom any correspondence should be addressed.

 © 2008 IOP Publishing Ltd Printed in the UK

ultrasonic waves to be transmitted, while the opaque zones serve to block the ultrasonic waves. A positive (negative) zone plate is defined as having a transparent (opaque) central zone. The radii of the zones are chosen such that the transmitted ultrasonic waves from zones for a particular wavelength λ tend to arrive in-phase on the zone plate's symmetric axis z at a predetermined focus z_0, and these ultrasonic waves will constructively interfere at the focal point. The radii r_n of the alternating zones are determined from the Fresnel diffraction theory and are given by [18]

$$r_n^2 = n\lambda\left(z_0 + \frac{n\lambda}{4}\right) \qquad n = 1, 2, 3, \ldots, \tag{1}$$

where z_0 is the focal length, and λ is the acoustic wavelength in the medium in which the device is located. A commonly used acoustic FZP can be made by depositing a zone plate electrode pattern on one face of a piezoelectric transducer while maintaining a full electrode on the opposite face. It is simple to construct the FZP by this method, but the destructively acoustic crosstalk between the zones is serious. In this paper, we use a piezoelectric PZT-5 transducer zone plate pattern, where the zones are separated by filling with sound-absorption materials between them to decrease the acoustic crosstalk, and the electrodes on one face of the transducer are the divided same zone plate pattern. The opposite face is given a full-face gold electrode. As an exploratory study, we have built a two-zone ultrasonic FZP transducer. We use the second and the fourth zone plates, the radius of the zone plate pattern is designed according to equation (1).

2. Materials and methods

2.1. Imaging principle

The purpose of PA imaging is to reconstruct the optical absorption distribution of tissue by detecting PA signals generated by absorption of pulsed light by tissue chromophores. Based on the studies of Xu *et al* [19] and Wang *et al* [20], the projections of optical absorption distribution can be obtained directly by deconvolving the recorded PA signal originating from a point source outside the sample. PA signals from a point source can be easily measured by focusing the incident laser on an absorber surface to form a point source. The approach allows the optical absorption distribution to be reconstructed without knowing the impulse response of the transducer which is difficult to measure in practice.

Before the signals detected by the zone plate areas can be processed, they have to be corrected according to their time delays. Similar to B-mode ultrasound received beamforming, the signals are delayed to create constructive interference at each imaging depth. Figure 1 shows the time delays Δt_2 and Δt_4, which appear when a signal travels from a source located on-axis to the second and the fourth zone plate, respectively. The time delay applied to the ith zone plate can be expressed as

$$\Delta t_i = \frac{\sqrt{z^2 + R_i^2} - z}{v}, \tag{2}$$

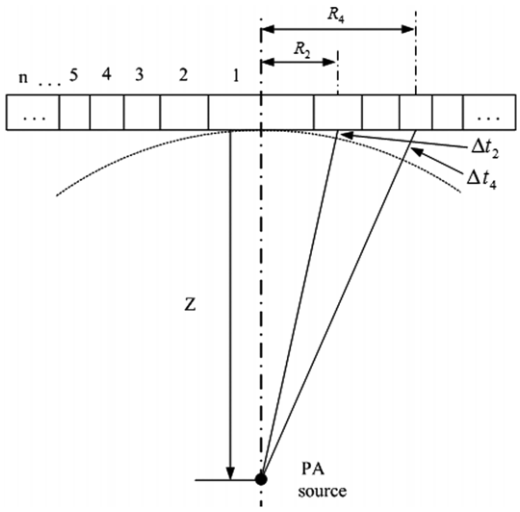

Figure 1. Time delays in arrival of signals generated by a PA source located on-axis at the second zone plate (Δt_2) and the fourth zone plate (Δt_4).

where R_i is the distance from the symmetric axis of the zone plates to the centre of the ith zone plate detection area, z is the depth of the PA source to the transducer and v is the velocity of sound. This procedure is analogous to dynamic focusing in ultrasound imaging. Since the time axis of zones are corresponding to the depth of the PA source by applying this time delay, the delayed signals of zones can be summed as

$$S(t) = \sum_{i=1}^{N} S(i, t - \Delta t_i), \tag{3}$$

where $S(i, t)$ is the received PA signal at the ith zone plate, Δt_i is the time delay applied to it and N denotes the total number of zone plates included in the summation.

To improve imaging quality, we utilize the signal coherence level factor as the weight factor of the summed signals. The coherence of the delayed signals included in the summation is estimated by the modified coherence factor (CF) [21], which is defined as

$$\mathrm{CF}(t) = \left|\sum_{i=1}^{N} S(i, t - \Delta t_i)\right|^2 \Big/ \sum_{i=1}^{N} |S(i, t - \Delta t_i)|^2. \tag{4}$$

The numerator in equation (4) represents the energy of the coherent signal sum, and the denominator denotes the total incoherent energy of the delayed signals included in the sum. According to the definition, the CF is a real quantity ranging from 0 to N. The CF is maximal when the delayed signals are identical (i.e. perfectly interfere); this is the case where the PA source is in the symmetrical axis of the zone plates. In other words, the CF of an on-axis PA source without focusing errors is high. The CF is low in the case that the PA source is not on the symmetrical axis since a destructive summation occurs in the numerator of equation (4). A high CF indicates that the image intensity should be enhanced, while a low one indicates that the image intensity should be reduced. Therefore, the CF can be used as a focusing-quality index for the beam focusing, and the resolution on the scanning direction can be improved.

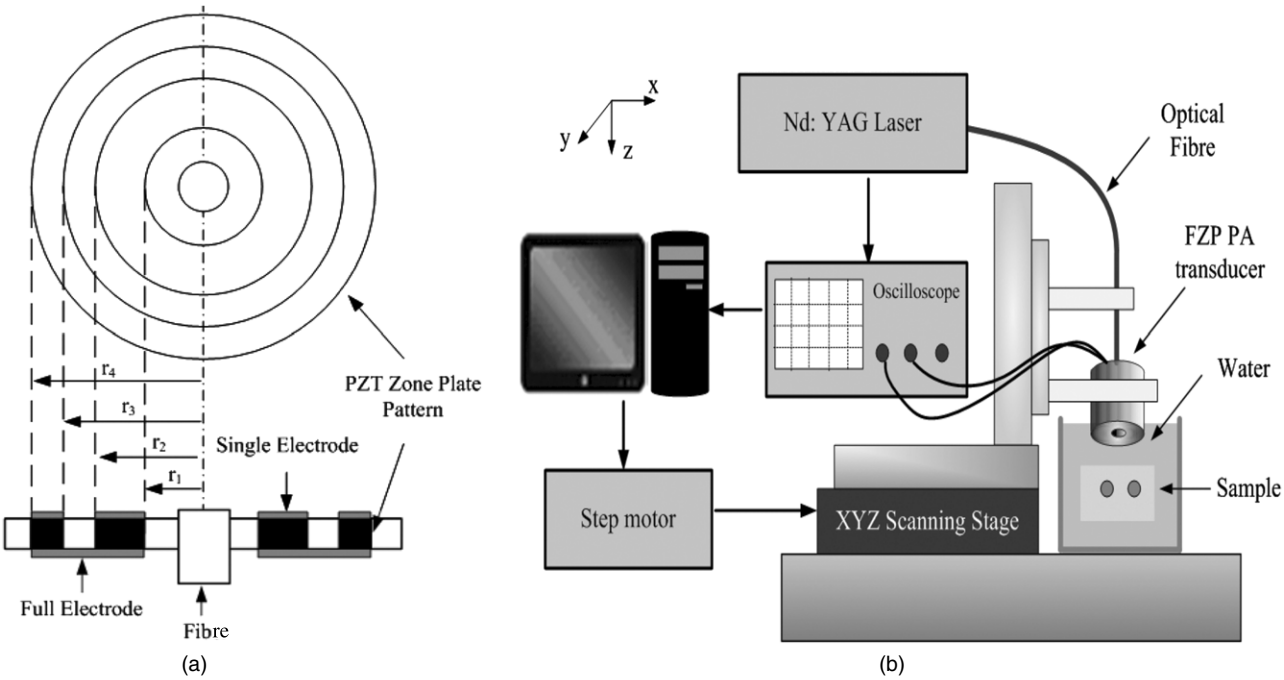

Figure 2. (*a*) The PA two-zone FZP transducer: cross-section along axis and the PZT zone plate pattern of the transducer. (*b*) The PA imaging system using the FZP PA transducer.

Based on this property, a coherence-factor weighting (CFW) technique can be developed to further improve the focusing quality of the FZP transducer. The CF-weighted signal, SW(t) can be expressed as

$$\mathrm{SW}(t) = S(t) \cdot \mathrm{CF}(t). \tag{5}$$

Note that the CFW is performed at each imaging point. Because measurement noise is generally incoherent, the CFW technique can also improve the signal-to-noise ratio (SNR) of the PA signals.

Consequently, the PA image reconstruction is accomplished by (1) summing the time-delayed signals detected by the zone plate areas and calculating the CF of these signals; (2) calculating CF-weighted projection signal at each scanning point; (3) correcting the CF-weighted projection signal based on the Monte Carlo simulation for the optical attenuation in depth and back projecting it over arcs [22, 23] and (4) summing the back projections. Due to the directivity of the transducer, there is a receiving solid angle along the acoustic axis of the transducer. Therefore, the CF-weighted signals are back projected over a limited-angle arcs along the acoustic axis which is defined as the limited-field back-projection algorithm to reconstruct the PA image [2, 24].

2.2. Experimental system

The schematic diagram of the PA two-zone FZP transducer is shown in figure 2(*a*). The ultrasonic two-zone FZP transducer consists of two concentric ring-shaped PZT, which is axially electrically polarized. The design radii of the concentric zones are calculated via equation (1) using a chosen focal length of 10.0 mm at the central frequency of 2.0 MHz. This results in the following zone-boundary radii: $r_1 = 2.76$, $r_2 = 3.94$, $r_3 = 4.87$, $r_4 = 5.68$. The front electrodes are glued to one face of the two-zone transducer, and the opposite face is given a full-face back electrode. The sound-absorbing materials are filled around the ring-shaped PZT to avoid crosstalk between the zones, and the transducer is embedded in a brass housing to shield the electronics from electromagnetic noise.

The schematic of the experimental setup is shown in figure 2(*b*). A Q-switched Nd : YAG laser with a wavelength of 1064 nm, a pulse width of 6 ns at 40 mJ pulse^{-1} and a repetition rate of 15 Hz was used to generate PA signals. The light was coupled to an optical fibre (core diameter 600 μm), which was placed in the centre of the transducer to deliver light pulses to the sample. The sample was placed in a container filled with water. The transducer was mounted in an X–Y–Z scanning system to scan over the sample, and it was also immersed in water to ensure a good acoustical coupling. A dual-channel, digital oscilloscope (TDS3032-Tektronix) was used to collect PA signals at a sampling rate of 250 Msamples s^{-1}.

3. Results and discussion

3.1. Focal characteristics of FZP transducer

The key characteristic parameters of an acoustic zone plate transducer include focal length, depth of focus and beam width. As applied to ultrasound imaging, the beam width ultimately determines the achievable resolution in the transverse direction, and the depth of focus determines the achievable imaging range. Quantitative assessments of the focal length and depth of focus can be obtained from the relative pressure distribution or beam profile on the axis of cylindrical symmetry for the zone plate. Likewise, quantitative assessments of beam width can be made from the focal plane beam profile.

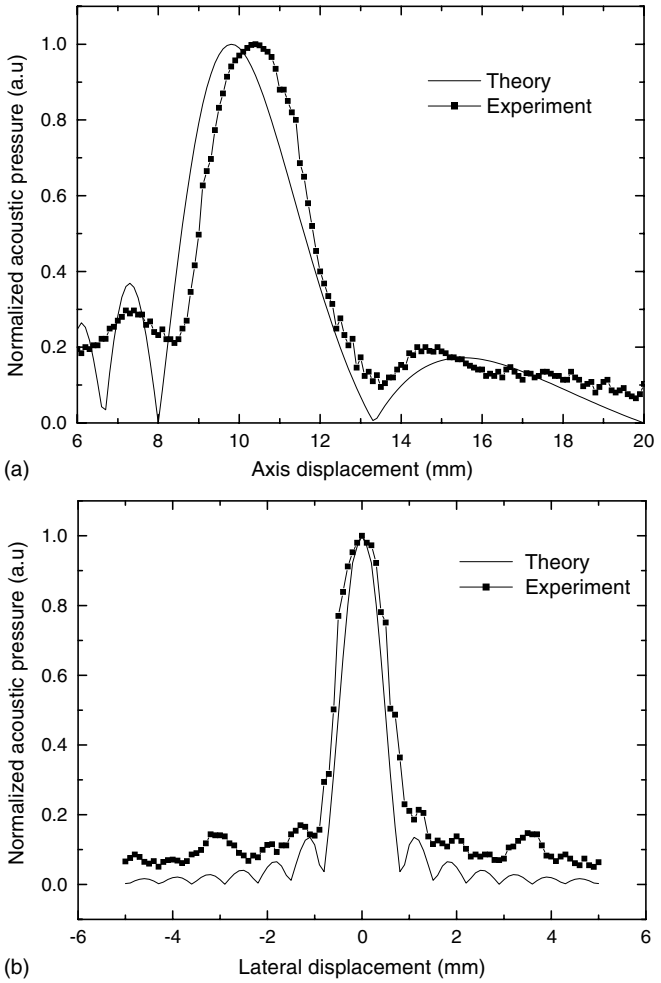

Figure 3. (*a*) Theoretical and experimental on-axis pressure profiles for the two-zone FZP transducer. (*b*) The theoretical and experimental focal plane profiles for the two-zone FZP transducer.

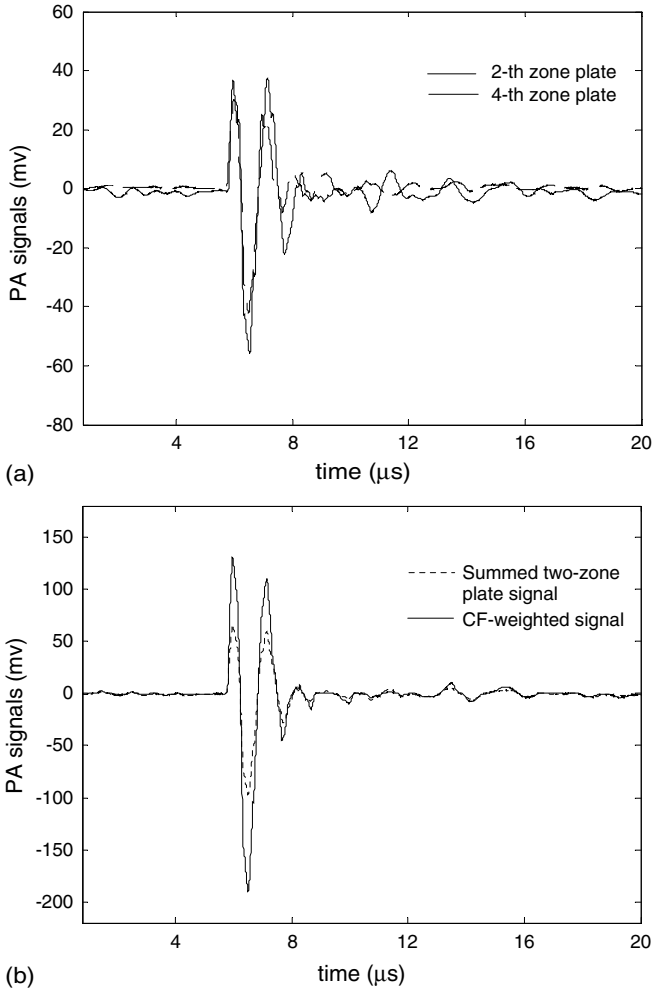

Figure 4. (*a*) The signals of a PA source located on the focal point of the FZP transducer detected by the two-zone plates of the transducer. (*b*) The summed two-zone-plate time-delayed signal (----) and the CF-weighted summed signal (——).

Based on the acoustic wave propagation theory and Huygens' principle, the acoustic field distribution can be calculated [16, 25]. To calculate the acoustic pressure distribution, the zone plate is modelled as a series of concentric, ring-shaped radiators mounted on a rigid baffle. All radiators are assumed uniformly excited with equal amplitude and in phase. Thus, all the zones vibrate only in the uniform thickness mode. The calculated normalized axis acoustic pressure distribution is shown in figure 3(*a*). It can be seen from figure 3(*a*) that the acoustic field is focused at a distance of 10 mm on the axis of the FZP transducer with a depth of focus of 3 mm, which means that the imaging range is about 3 mm. The theoretical calculated focal plane profile is shown in figure 3(*b*). The full width at half maximum (FWHM) of this profile is 0.94 mm.

The beam profiles were assessed by measuring the transmit field acoustic pressure distribution of the FZP transducer. The zones were excited with short 2 MHz sine wave. The acoustic field measurements were taken by scanning a commercial PVDF hydrophone with a diameter of 0.1 mm element in a tank containing de-ionized water. In order to locate the focal plane for the FZP transducer, the hydrophone was first scanned along the z axis to find the axial maximum and then in the x–y plane to find the true maximum in this plane. The actual focal length was determined to be 10.5 mm on the z axis for the zone plate transducer as shown in figure 3(*a*), and the actual depth of focus was about 3 mm. Once the focal point was located, one-dimensional scans in the focal plane were carried out. The measured focal plane profile is shown in figure 3(*b*) for comparison. The shapes of both profiles are very similar, with a little discrepancy between the amplitude of the pedestal in the experimental measurement and the theoretical prediction, and it may be caused by the ground noise of the system.

3.2. The CFW technique

The CFW technique is developed to further improve the focusing quality of the FZP transducer. The CF is used as the weight factor of the summed signals, as illustrated in figure 4 with the signals from the PA sources located on the focal point of the FZP transducer. The time-delayed PA signals from the original signals detected by the second zone plate and the fourth zone plate of the transducer are shown in figure 4(*a*), these time-delayed signals perfectly interfere, and the summed

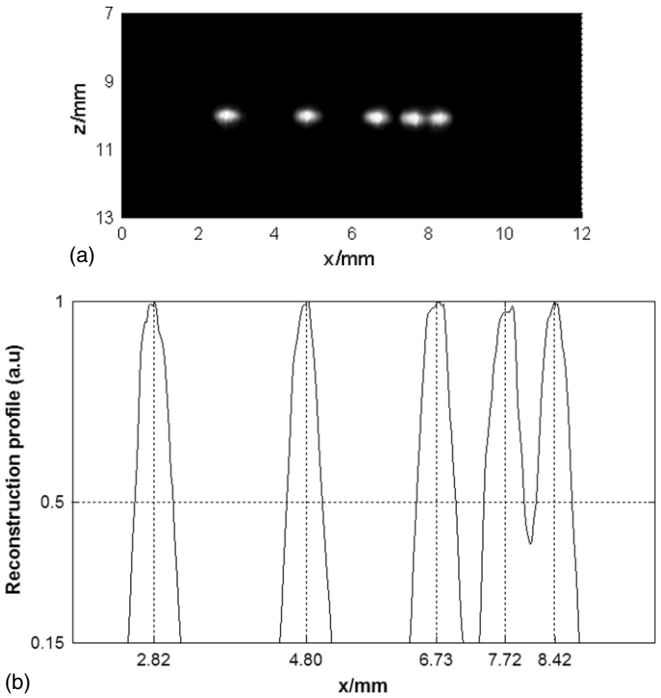

Figure 5. (*a*) The PA imaging for measuring the lateral resolution of this system. (*b*) The line profile of the reconstructed image shown in (*a*) with $z = 10.2$ mm.

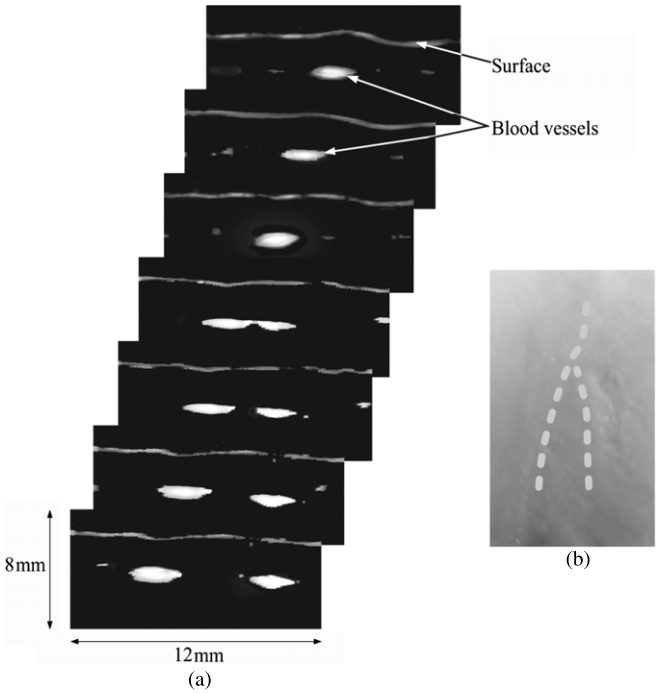

Figure 6. (*a*) PA image of two joining artificial blood vessels embedded in chicken breast tissues, which consists of seven slices with 2 mm distance apart. Horizontal axis: scan direction (mm); vertical axis: depth (mm). Each slice consisted of 61 measurement positions, with a space of 0.2 mm. (*b*) Photograph of measured area, the course of the vessels is indicated with dashed lines.

signal is also shown in figure 4(*b*) (dashed curve). It can be seen that the signals from the PA sources located on the focal point of the FZP transducer detected by the zone plate detection areas can interfere constructively. Thus, the CF is high in this case, the amplitude of the summed signal is enhanced after using the CF-weighted index, and it is clearly shown in figure 4(*b*) (solid curve). Otherwise, the CF is low in the case that PA sources are not on the symmetrical axis of the transducer since a destructive summation occurs; the amplitude of the summed signal is reduced after using the CF-weighted index. Therefore, the CF can be used as a focusing-quality index for the beam focusing, and the resolution on the scanning direction can be improved. Furthermore, the results show that the CFW technique has improved the SNR of the summed signal by 7 dB. Here, the SNR is defined as the difference between the maximal amplitude of the signal and the average noise amplitude.

3.3. The resolution of the imaging system

To evaluate the imaging resolution of the designed system, we imaged five graphite lines (0.1 mm in diameter) fixed in turbid phantom, which was made of 14.5% gelatin, and 85.5% water. The five graphite lines were parallel to each other at the same depth in turbid phantom with decreasing distance, so that they can be scanned by the transducer on a line, and the scanning line of the transducer was perpendicular to the graphite lines. The reconstructed PA image is shown in figure 5(*a*), the vertical distance from the scanning line of the transducer to the graphite lines is 10.2 mm, which is in the focal range of the FZP transducer. The minimum distance between two lines (the right-hand side in figure 5(*a*)) is 0.7 mm. The line profile of the reconstructed image shown in figure 5(*a*) with $z = 10.2$ mm is shown in figure 5(*b*). The lateral resolution, defined by the FWHM of the main lobe, is approximately 0.65 ± 0.015 mm (standard error). In figure 5 the low limit of the greyscale was set to 15% of the maximum value, making all the greyscale below this value appear black in the image. This low threshold was maintained in the following images.

3.4. Two-dimensional (2D) PA imaging

To demonstrate the ability of the FZP PA imaging system to image biological phantoms, the first experiment was performed with the two joining artificial blood vessels embedded in chicken breast tissues. Two silicone rubber tubes filled with undiluted human blood acted as the artificial blood vessels. The sample was in water with the distance of about 10.5 mm from the transducer to the blood vessels. The larger vessel (vessel on the left side in the PA image) has an inner diameter of 1.5 mm, and the smaller vessel on the right side has an inner diameter of 1.0 mm. The depth position of the vessels with respect to the chicken breast tissue surface is about 2.5 mm. The reconstruction PA imaging is shown in figure 6(*a*), and (*b*) shows the photograph of the scanned area. It can be seen that the cross-section of the blood vessels can be imaged clearly with high contrast, even the joined location of the vessels. Due to the difference in optical absorption between the water and the tissue, the tissue surface is also visible in images. Here, the optical attenuation in depth is corrected based on the Monte Carlo simulation [22]. The dimensionless optical fluence in homogenized chicken breast tissue as a function of depth is computed from the Monte Carlo simulation. In

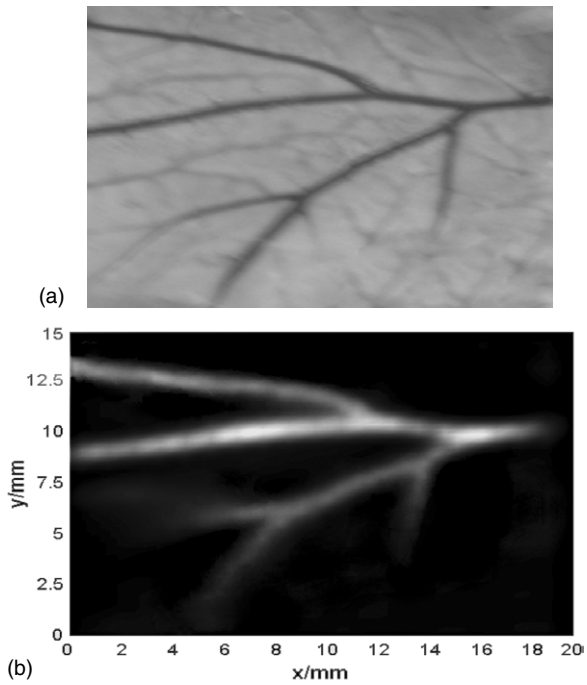

Figure 7. (*a*) Photograph of the imaged area of the blood vessels of chicken embryo CAM. (*b*) The MAP PA image of CAM *in vitro*.

the simulation, the optical parameters are refractive index $n = 1.37$, absorption coefficient $\mu_a = 0.1\,\mathrm{cm}^{-1}$, scattering coefficient $\mu_s = 20\,\mathrm{cm}^{-1}$ and anisotropy factor $g = 0.9$ [23]. Thus, the projection signal can be corrected based on the computed optical fluence along the depth.

The image consisted of seven vertical slices, with a space of 2 mm between each slice along the blood vessels. Each slice consisted of 61 measurement positions, with a step of 0.2 mm. At each measurement position the PA signals were measured, and the signals were averaged 16 times to enhance the SNR. This approach provided a 2D PA image (in depth and lateral) for each scan line. The total scan time was 15 min. It can be seen that the shape of the cross-sectional images of the blood vessels to be slightly broaden in the lateral direction. This is caused mainly by the limited lateral resolution of the imaging system.

To further verify the ability of the imaging system to image the network of blood vessels, the second experiment was performed with the blood vessels of chicken embryo chorioallantoic membrane (CAM) figure 7. The blood vessels of CAM were imaged using the maximum amplitude projection (MAP) along the z axis to the x–y plane (imaging plane) [4]. Here, the MAP image was formed by projecting the maximum PA amplitudes along the direction to the orthogonal imaging plane. A 2D scan over a 15 mm × 20 mm area was taken with a step of 0.2 mm by the FZP transducer with the distance of 10.5 mm to the blood vessels sample. The diameter of the main blood vessels ranged from 0.1 to 0.6 mm. It can be seen that the main structure of the blood vessels is clearly imaged with high contrast. However, some microvessels are not visible in the image, and this is caused by the limited frequency band response of the transducer.

To improve the focusing equality of the FZP transducer and to further improve the imaging resolution, we applied the CFW technique to the projection signals. However, the resolution of our present imaging system is not high enough to image the microvessel. If more zone plates and the high frequency wider bandwidth piezoelectric materials are used, the imaging system based on the FZP transducer will have the potential to be developed as PA microscopy for *in vivo* imaging.

4. Conclusion

The PA imaging system based on an ultrasonic FZP transducer is successfully used for imaging the blood vessels of chicken embryo CAM with the MAP. The limited-field back-projection deconvolution algorithm combined with the CFW technique is used to reconstruct 2D PA images of two joining artificial blood vessels embedded in chicken breast tissues, which agree well with the samples. Perspective application of this system is to localize and monitor neovascularization in tumour angiogenesis, but the lateral resolution needs to be improved.

Acknowledgments

This research is supported by the National Natural Science Foundation of China (30470494; 30627003) and the Natural Science Foundation of Guangdong Province (7117865).

References

[1] Wang X D, Pang Y J, Ku G, Stoica G and Wang L V 2003 Three dimensional laser-induced photoacoustic tomography of mouse brain with the skin and skull intact *Opt. Lett.* **28** 1739–41

[2] Yang D W, Xing D, Gu H M, Tan Y and Zeng L M 2005 Fast multielement phase-controlled photoacoustic imaging based on limited-field-filtered back-projection algorithm *Appl. Phys. Lett.* **87** 194101

[3] Yang D W, Xing D, Tan Y, Gu H M and Yang S H 2006 Integrative prototype B-scan photoacoustic tomography system based on a novel hybridized scanning head *Appl. Phys. Lett.* **88** 174101

[4] Zhang H F, Maslov K, Stoica G and Wang L V 2006 Functional photoacoustic microscopy for high-resolution and noninvasive in vivo imaging *Nature Biotechnol.* **24** 848–51

[5] Kolkman R G M, Hondebrink E, Steenbergen W and de Mul F F M 2003 *In vivo* photoacoustic imaging of blood vessels using an extreme-narrow aperture sensor *IEEE J. Sel. Top. Quantum Electron* **9** 343–6

[6] Siphanto R I, Thumma K K, Van Leewen T G, de Mul F F M, van Neck J W, van Adrichem L N A and Steenbergen W 2005 Serial noninvasive photoacoustic imaging of neovascularization in tumor angiogenesis *Opt. Express* **13** 89–95

[7] Oraevsky A A, Savateeva E V, Solomatin S V, Karabutov A A, Andreev V G, Gatalica Z, Khamapirad T and Henrichs P M 2002 Optoacoustic imaging of blood for visualization and diagnostics of breast cancer *Proc. SPIE* **4618** 81–94

[8] Ermilov S A, Coniusteau A, Mehta K, Lacewell R, Henrichs P M and Oraevsky A A 2006 128-channel laser optoacoustic imaging system for breast cancer diagnostics *Proc. SPIE* **6086** 608609

[9] Zhang H F, Maslov K, Sivaramakrishnan M, Stoica G and Wang L V 2007 Imaging of hemoglobin oxygen saturation variations in single vessels *in vivo* using photoacoustic microscopy *Appl. Phys. Lett.* **90** 053901
[10] Yang S H, Xing D, Lao Y Q, Yang D W, Zeng L M, Xiang L Zh and Chen W R 2007 Noninvasive monitoring of traumatic brain injury and post-traumatic rehabilitation with laser-induced photoacoustic imaging *Appl. Phys. Lett.* **90** 243902
[11] Yang S H, Xing D, Zhou Q, Xiang L Zh and Lao Y Q 2007 Functional imaging of cerebrovascular activities in small animals using high-resolution photoacoustic tomography *Med. Phys.* **34** 3294–301
[12] Xiang L Zh, Xing D, Gu H M, Yang D W, Yang S H and Zeng L M 2007 Real-time optoacoustic monitoring of vascular damage during photodynamic therapy treatment of tumor *J. Biomed. Opt.* **12** 014001
[13] Yamazaki M, Sato S, Ashida H, Saito D, Okada Y and Obara M 2005 Measurement of burn depths in rats using multiwavelength photoacoustic depth profiling *J. Biomed. Opt.* **10** 064011
[14] Zhang H F, Maslov K, Stoica G and Wang L V 2006 Imaging acute thermal burns by photoacoustic microscopy *J. Biomed. Opt.* **11** 054033
[15] Born M and Wolf E 1999 *Principles Of Optics* 7th edn (Cambridge: Cambridge University Press)
[16] Sleva M Z, Hunt W D and Briggs R D 1994 Focusing performance of epoxy- and air-backed polyvinylidene fluoride Fresnel zone plates *J. Acoust. Soc. Am.* **96** 1627–33
[17] Schindel D W, Bashford A G and Hutchins D A 1997 Focussing of ultrasonic waves in air using a micromachined Fresnel zone-plate *Ultrasonics* **35** 275–85
[18] Wade G 1976 *Acoustical Imaging* (New York: Plenum)
[19] Xu M H, Xu Y and Wang L V 2003 Time-domain reconstruction algorithms and numerical simulations for thermoacoustic tomography in various geometries *IEEE Trans. Biomed. Eng.* **50** 1086–99
[20] Wang Y, Xing D, Zeng Y G and Chen Q 2004 Photoacoustic imaging with deconvolution algorithm *Phys. Med. Biol.* **49** 3117–24
[21] Liao C K, Li M L and Li P C 2004 Optoacoustic imaging with synthetic aperture focusing and coherence weighting *Opt. Lett.* **29** 2506–8
[22] Wang L V, Jacques S L and Zheng L Q 1995 MCML-Monte Carlo modeling of light transport in multi-layered tissues *Comput. Methods Programs Biomed.* **47** 131–46
[23] Marquez G, Wang L V, Lin S P, Schwartz J A and Thomsen S L 1998 Anisotropy in the absorption and scattering spectra of chicken breast tissue *Appl. Opt.* **37** 798–804
[24] Yang D W, Xing D, Yang S H and Xiang L Z 2007 Fast full-view photoacoustic imaging by combined scanning with a linear transducer array *Opt. Express* **15** 15566–75
[25] Weyns A 1980 Radiation field calculations of pulsed ultrasonic transducers: I. Planar circular, square and annular transducers *Ultrasonics* **18** 183–8